A&A 647, A47 (2021)
https://doi.org/10.1051/0004-6361/202039729

Astronomy & Astrophysics

Astrophysical properties of newly discovered Magellanic Cloud star clusters

Andrés E. Piatti[1,2]

[1] Instituto Interdisciplinario de Ciencias Básicas (ICB), CONICET-UNCUYO, Padre J. Contreras 1300, M5502JMA Mendoza, Argentina
e-mail: andres.piatti@unc.edu.ar
[2] Consejo Nacional de Investigaciones Científicas y Técnicas (CONICET), Godoy Cruz 2290, C1425FQB Buenos Aires, Argentina

Received 20 October 2020 / Accepted 23 December 2020

ABSTRACT

New star cluster candidates projected toward the Large and Small Magellanic Clouds (LMC, SMC) have been recently discovered from relatively deep imaging surveys. Here, we conduct a sound analysis of 24 star cluster candidates located in the outer regions of the LMC and SMC using point spread function photometry produced by the Survey of the Magellanic Stellar History. With only one exception, the studied objects were shown to be genuine stellar aggregates. We drew our conclusions on their physical characteristics once their observed color-magnitude diagrams (CMDs) were statistically decontaminated by the presence of field stars. The resulting cleaned CMDs, for stars with assigned membership probabilities higher than 50%, were compared with synthetic CMDs generated for thousands of combinations of ages, distances, metallicities, star cluster masses, and binary fractions. The parameters of the best-matched synthetic CMDs obtained from a likelihood approach were adopted as the star cluster astrophysical properties. The present star cluster sample spans a wide range of distances, from those star clusters located in front of the LMC through those along the onset of the Magellanic Bridge up to those behind the SMC. Their ages reveal different formation episodes that took place over the course of galaxy formation and others as a consequence of interactions among galaxies. From their estimated metallicities and ages, we speculate on the possibility that relatively metal-deficient gaseous flows have existed between these galaxies during nearly the last one Gyr ($\log(\mathrm{age\,yr^{-1}}) \approx 9.0$), which facilitated the formation of young star clusters in the galaxy peripheries. Despide the LMC-SMC interactions, the studied star clusters are similar or more massive than their counterparts in the Milky Way, suggesting that tidal effects are relatively more important in our Galaxy.

Key words. methods: observational – techniques: photometric – Magellanic Clouds – galaxies: star clusters: general

1. Introduction

Recent imaging surveys of the Magellanic Clouds (MCs) have allowed the community to embark on searches of relatively compact, small, and poorly populated star clusters (see Table 1 in Maia et al. 2019). Visual inspections of images (e.g., Bica et al. 2020) and machine-learning techniques (e.g., Cerny et al. 2020) have both revealed the existence of stellar overdensities proposed as star clusters spread throughout the surveyed areas. Several of these star cluster candidates have not been confirmed as genuine physical systems (Piatti et al. 2014; Piatti 2018a), while others have turned out to be star clusters with properties that defy our prior knowledge about the formation, structure, dynamics, and chemical evolution of the Magellanic Clouds (Piatti et al. 2016, 2018a; Gatto et al. 2020).

By using wide-field high-quality images released from the Survey of the Magellanic Stellar History (SMASH; Nidever et al. 2017), Piatti (2017) used density kernel estimators with physically meaningful bandwidths to detect the smallest or less dense star clusters in the Magellanic Clouds. This study found 24 new star cluster candidates (see his Table 1), most of them located in the outer regions of both Clouds, thus reinforcing previous suggestions that those regions were not as carefully explored in the past. Their fundamental parameters were not estimated, which means that the verified status of these candidates as stellar aggregates still needs to be confirmed. The SMASH DR2 is now publicly available from the portal of the Astro Data Lab[1], which is part of the Community Science and Data Center of NSF's National Optical Infrared Astronomy Research Laboratory. As a result, we have now a chance to study these candidates in detail, providing, for the first time, their astrophysical properties. The SMASH is a community Dark Energy Camera (DECam) survey of the Magellanic Clouds, mapping 480 deg^2 (distributed over ∼2400 deg^2 at ∼20% filling factor, which complements the 5000 deg^2 Dark Energy Survey's partial coverage of the Magellanic periphery) to ∼24th mag *griz* (and *u* ∼23), with the goal of identifying broadly distributed, low-surface-brightness stellar populations associated with the stellar halos and tidal debris of the Magellanic Clouds. The SMASH will also derive spatially-resolved star-formation histories covering all ages out to large radii of the MCs that will further complement our understanding of their formation. DECam is a wide-field optical imager (FOV = 2.2×2.2 deg^2, scale = 0.263 arcsec pix^{-1}) attached to the Cerro Tololo Interamerican Observatory Blanco 4 m telescope.

Beyond the usefulness of enlarging the sample of well-studied MC star clusters, the fact that Piatti (2017)'s new candidates are located in the outer regions of both MCs is of particular interest. The outer regions of the Large and Small Magellanic Clouds (LMC, SMC) have been primary scenarios of

[1] https://datalab.noao.edu/smash/smash.php

the interaction between both galaxies, namely: star clusters were stripped off (Carpintero et al. 2013); new stars clusters formed (Piatti et al. 2018b); and ancient star clusters were believed to have been found (Piatti et al. 2019). Hence, star clusters located in these regions challenge our ability to disentangle the early star cluster formation episodes from more recent formation events. Such a distinction is necessary for a better understanding of the age-metallicity relationships and metallicity gradients observed in these galaxies (Piatti & Geisler 2013).

In this work, we analyze SMASH data sets for the 24 star cluster candidates identified by Piatti (2017). Section 2 deals with the decontamination of the color-magnitude diagrams (CMDs) from field star contamination and the estimate of ages, distances, and metallicities. The implications of the resulting parameters in the context of the formation and interaction of both Magellanic Clouds are discussed in Sect. 3. Finally, Sect. 4 summarizes the main conclusions of this work.

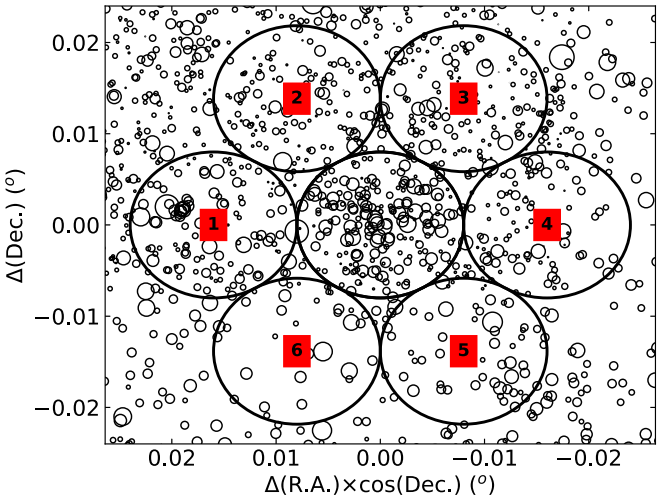

Fig. 1. Schematic chart centered on Field 16−02. The size of the symbols is proportional to the g brightness. The radius of the superimposed circles equals the adopted cluster's radius (see Table 1). Six labeled reference star fields distributed around the star cluster circle are also given.

2. Fundamental parameters of star clusters

2.1. Cleaning the color-magnitude diagrams

We retrieved RA and Dec coordinates, PSF g, i magnitudes and their respective errors, $E(B-V)$, interstellar reddening, and χ and SHARPNESS parameters of stellar sources distributed within circles with radii of 6′ (the star cluster candidates are smaller than ∼0.3′) from the Astro Data Lab. In order to assure the selection of point sources, we applied the following filters: $0.2 \leq \text{SHARPNESS} \leq 1.0$ and $\chi < 0.5$, so cosmic rays, bad pixels, galaxies, and unrecognized double stars were excluded. The SHARPNESS and χ are image quality diagnostic parameters used by DAOPHOT.

We carefully monitor the contamination of field stars in the star cluster CMDs by using six different star-field CMDs built from stars distributed in circular areas of equal size as the cluster area distributed around it (see Fig. 1). This is because the star field varies in stellar density as well as in the distribution of brightness and color of its stars from one place to the other. The chosen regions are meant to include any possible star-field population and reddening variation around the star clusters. Because the star cluster candidates are relatively small and would seem to contain a relative small number of stars (see Fig. 3 in Piatti 2017), we decided to clean cluster areas with radii slightly larger than the readily visible cluster dimensions. Thus, we minimize the presence of potential residuals from the cleaning procedure when building the cleaned star cluster CMDs.

Field star contamination plays an important role when analyzing Magellanic Cloud star cluster CMDs. Because of the galactocentric distances of both galaxies, star cluster and field star sequences in the CMDs can be superimposed. This means that it is not a straightforward exercise to consider a star a cluster member from its lone position in the CMD. In some cases, such an ambiguity can be solved on the basis of additional information related to the proper motions, radial velocities, or chemical abundances of individual stars Unfortunately, in the case of our star cluster candidates, *Gaia* DR2 proper motions (Gaia Collaboration 2016, 2018) are unavailable for several stars concentrated in very small regions or they are unreliable because of their apparent low brightness. It is for this reason that we exploit the photometry of reference field stars to decontaminate the star cluster CMDs.

In general terms, the reference star field is placed adjacent to the star cluster field, but not too far from it, so that it can be a suitable representative of the star field projected along the line of sight (LOS) of the star cluster. Frequently, we must adopt the assumption of homogeneity in the stellar density and in the distribution of luminosities and effective temperatures of field stars across the star cluster field and around. This means that field stars located along the LOS of the star cluster can mimic astrophysical properties to those located along a direction slightly shifted from the LOS and toward the star cluster. However, even though the star cluster is not projected onto a crowded star field or is not affected by differential reddening, it is highly possible that we might find differences throughout the star cluster's surrounding field. Bearing in mind the above considerations, we decided to clean the star field contamination in the star cluster CMDs by using the six different devised reference star-field areas described above at one time.

We followed three main steps while decontaminating the star cluster CMDs. On the one hand, we properly represent each reference star field by simultaneously considering its stellar density and the observed distribution of its stars in luminosity and effective temperatures (number of stars per CMD mag and color units). Then we statistically subtract the reference star field from the star cluster CMD. Finally, we assign membership probabilities from the consideration of the six different resulting cleaned star cluster CMDs (one cleaned CMD per reference star field CMD). Stars with relatively high membership probabilities that are located along a single theoretical isochrone (corresponding to an age, distance, and metallicity) are considered cluster members. This method was devised by Piatti & Bica (2012) and successfully used in other studies to decontaminate CMDs of star clusters projected onto crowded fields in the Milky Way and the MCs (see, e.g., Piatti et al. 2016, 2020; Piatti 2018b, and references therein).

We subtract, from the star cluster CMD, a number of stars that is equal to that of the reference star field. When we subtracted fewer stars or more stars, respectively, we were able to confirm the presence of a more populous object or the absence of a real aggregate. The distribution of magnitudes and colors of the subtracted stars ought to, in addition, resemble that of the reference star field. With the aim of avoiding stochastic effects caused by very few field stars distributed in less-populated CMD regions, appropriate ranges of magnitudes and colors around the

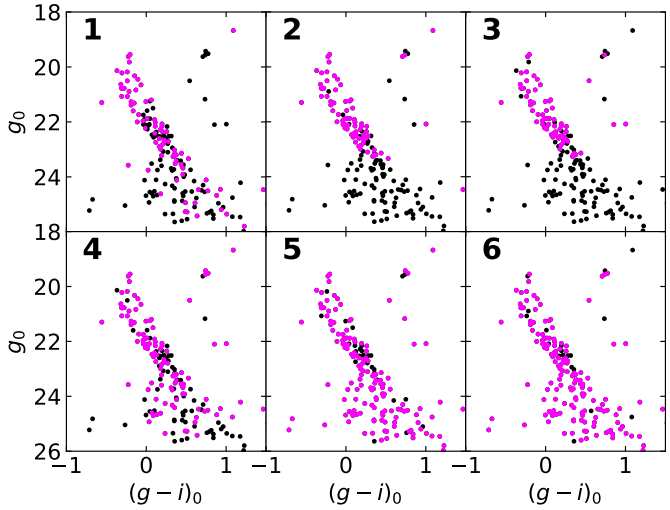

Fig. 2. Color-magnitude diagram of Field 16−02. Black points represent all the measured stars located within the cluster radius. Magenta points represent the stars that remained unsubtracted after the CMD cleaning procedure. The reference star field used to decontaminate the star cluster CMD is indicated at the top-left margin (see also Fig. 1).

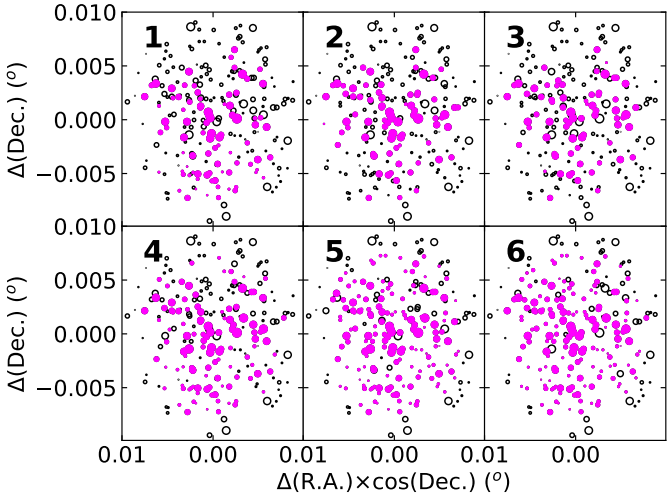

Fig. 3. Chart of the stars in the field of Field 16−02. The size of the symbols is proportional to the g brightness of the star. Open black circles represent all the measured stars located in the cluster circle. Filled magenta circles represent the stars that remained unsubtracted after the CMD cleaning procedure. The reference star field used to decontaminate the star cluster CMD is indicated at the top-left margin (see also Fig. 1).

CMD positions of field stars ought to be used. Thus, finding a star in the star cluster CMD with a magnitude and color within those boundaries close to the magnitude and color of each field star is highly probable. In the case where there is more than one star located inside that delimited CMD region, the closest one to the center of that (magnitude, color) box is subtracted. We started here with boxes of $(\Delta g, \Delta(g-i)) = (2.0\,\mathrm{mag}, 1.0\,\mathrm{mag})$ centered on the magnitude and color values of each reference field star. We based our analysis on dereddened CMDs, so we first corrected by interstellar extinction the g and i magnitudes using the $E(B-V)$ values provided by SMASH and the $A_\lambda/E(B-V)$ ratios, for $\lambda = g,\ i$, given by Abbott et al. (2018). The photometric errors are also taken into account while searching for a star to be subtracted from the star cluster CMD. With that purpose, we iterate up to 1000 times the comparison between the magnitude and color of the reference field star and those of the stars in the star cluster CMD. If a star in the star cluster CMD falls inside the box defined for the reference field star, we subtract that star. The iterations are carried out by allowing the magnitude and color of the star in the star cluster CMD takes smaller or larger values than the mean ones according to their respective errors. Figure 2 illustrates the results of the decontamination of field stars using the six different reference star fields depicted in Fig. 1. The spatial distribution of these stars is shown in Fig. 3.

Finally, we assign a membership probability to each star that remain unsubtracted after the decontamination of the star cluster CMD. Because unsubtracted stars vary from one cleaned CMD to the other, we define the membership probability $P(\%) = 100 \times N/6$, where N represent the number of times a star was not subtracted during the 6 different CMD cleaning executions. Figure 4 illustrates the spatial distribution and corresponding CMD of stars measured in the field of the star cluster Field 16−02, painted according to their membership probabilities P. We applied the above cleaning procedure to the remaining 23 star cluster candidates discovered by Piatti (2017). The resulting cleaned star cluster CMDs and the respective spatial distributions of the measured stars are included in the Appendix A. We found that Field 30−02 is not, in fact, a real star cluster, but a chance grouping of stars.

2.2. Estimating star cluster fundamental parameters

At first glance, the cleaned star cluster CMDs reveal objects that appear to span young to moderately old ages. Because the age estimate depends on the star cluster's metallicity and distance, we employed routines of the Automated Stellar Cluster Analysis code (`ASteCA`, Perren et al. 2015) to derive all of them simultaneously. The `ASteCA` suite of tools is designed to analyze data sets of star clusters in order to determine their basic parameters. We thus obtain a synthetic CMD that best matches the star cluster CMD. The metallicity, age, distance, star cluster present mass, and binary fraction associated to that generated synthetic CMD are adoped as the best-fitting star cluster parameters.

We start by using the theoretical isochrones computed by Bressan et al. (2012) for the SMASH photometric system. We downloaded theoretical isochrones for different metallicity values, ranging from $Z = 0.000152$ ([Fe/H] = −2.0 dex) up to 0.030152 ([Fe/H] = 0.30 dex) in steps of $\Delta Z = 0.001$, thus covering almost the entire metallicity regime of the MCs (Piatti & Geisler 2013). This is an important consideration because the star clusters we study here lie in the outer regions of the LMC and the SMC, where metal-poor old and metal-rich young objects formed at the galaxy formation and galaxy interaction, respectively. As for their ages, we downloaded isochrones from $\log(\mathrm{age\,yr^{-1}}) = 6.0$ (1 Myr) up to 10.1 (12.5 Gyr) in steps of $\Delta\log(\mathrm{age\,yr^{-1}}) = 0.05$. In total, we gathered nearly 2500 different theoretical isochrones.

The input data sets consist in intrinsic magnitudes g_0 and dereddened colors $(g-i)_0$ for all the stars with membership probabilities $P \geq 50\%$, that is, all colored points in Figs. 4 and A.1–A.8, with their respective uncertainties. For generating the synthetic CMDs, we adopted the initial mass function of Kroupa (2002); a minimum mass ratio for the generation of binaries of 0.5; and a range of true distance moduli from 18.0 mag (40 kpc) up to 19.5 mag (80 kpc). We explore the parameter space of the synthetic CMDs through the minimization of the likelihood function defined by Tremmel et al. (2013) using a parallel tempering Bayesian MCMC algorithm. Errors in the obtained

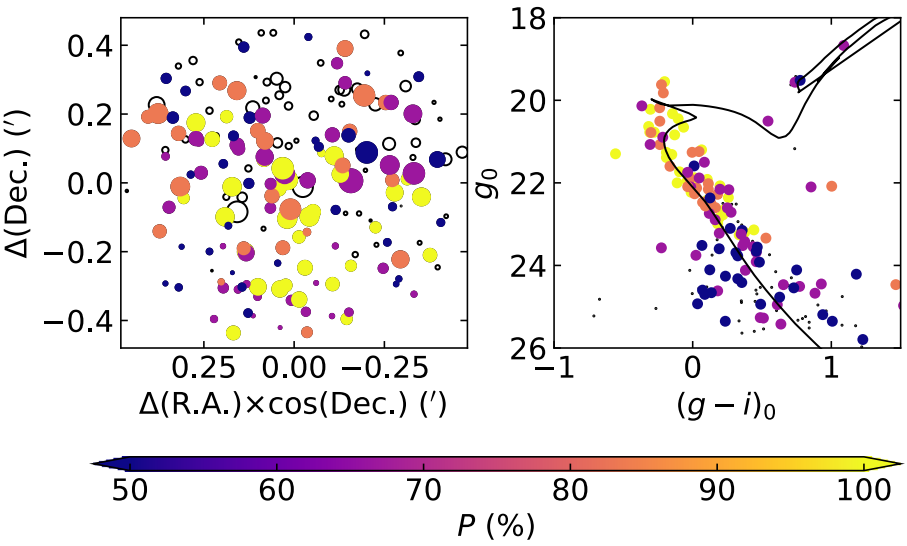

Fig. 4. Spatial distribution (*left panel*) and corresponding intrinsic CMD (*right panel*) of stars measured by SMASH in the field of Field 16−02. Symbols for stars with membership probabilities $P \geq 50\%$ are painted according to the color bar. The best-fitted theoretical isochrone is also superimposed in the cluster CMD.

parameters are estimated from the standard bootstrap method described in Efron (1982). We refer the reader to the work of Perren et al. (2015) for details concerning the implementation of these algorithms. Table 1 lists the resulting parameters for the entire star cluster sample. We illustrate the performance of the parameter matching procedure by superimposing the isochrone corresponding to the best-matched synthetic CMD to the cleaned star cluster CMDs (see, Figs. 4 and A.1–A.8).

3. Analysis and discussion

The advantage of playing with thousands of synthetic CMDs allows for a larger number of free parameters to be fitted. This is the case of the true distance modulus. In dealing with theoretical isochrones fitted to star cluster CMDs, a mean distance modulus is frequently adopted because the combination of the Magellanic Cloud distances with their respective LOS disk depths implies a variation of the distance moduli – all the while bearing in mind that any star cluster could be placed in front of or behind the LMC or SMC – of $\Delta(m-M)_0 \sim 0.2$ mag. The latter comes from considering for the LMC: $(m-M)_0 = 18.49 \pm 0.09$ mag (de Grijs et al. 2014) and $\langle \mathrm{LOS} \rangle = 3.44 \pm 1.16$ kpc (Subramanian & Subramaniam 2009) and for the SMC: $(m-M)_0 = 18.98 \pm 0.03$ mag (Graczyk et al. 2020) and $\langle \mathrm{LOS} \rangle = 6.0 \pm 1.7$ kpc (Crowl et al. 2001). This difference is much smaller than the difference in absolute magnitude between two closely spaced isochrones with $\Delta(\log(\mathrm{age\,yr^{-1}}) = 0.1$ (a typical age error), so that the adoption of a unique value for the distance modulus does not dominate the final error budget incurred in matching isochrones to the star cluster CMDs. However, the MCs are more extended than previously estimated, showing tidally-induced warps, substructures and tidal distortions in the peripheries, etc. (Mackey et al. 2016, 2017; Choi et al. 2018). Therefore, the use of the true distance modulus as a free parameter in the likelihood approach helps us to place the studied star clusters with greater accuracy.

The resulting spatial distribution of the studied star clusters is depicted in Fig. 5. For comparison purposes, we included as reference the positions of star clusters cataloged by Bica et al. (2008). They clearly delineate the bars, arms, outer disks, bridge, etc. As can be seen, the present star cluster sample consists of objects spread out across the outer regions of the LMC and SMC, and the Magellanic Bridge. The LMC star clusters span a narrower range of distances than those in the SMC, suggesting that the SMC is more elongated than the LMC along the LOS. This spatial pattern traced by star clusters is also seen from other galaxy components which show that the Magellanic Bridge along with its onset in the SMC (Piatti et al. 2015), connects both MCs (Wagner-Kaiser & Sarajedini 2017) and also show that the SMC is elongated along the LOS (Jacyszyn-Dobrzeniecka et al. 2017; Nidever et al. 2019; Massana et al. 2020). We point out that the novel picture of SMC star clusters spanning a range of ∼15 kpc in distance along the LOS would not have been disentangled if a mean distance modulus had been adopted while analyzing the star cluster CMDs.

The age estimates of these star clusters (see Fig. 6) are also worthy of discussion. In general terms, they confirm the outside-in formation scenario (Carrera et al. 2008; Meschin et al. 2014), which posits that metal-poor star clusters formed first and the youngest ones were born from the gas that collapsed to the innermost regions. Old star clusters that formed at the core of the galaxy had more chances to be disrupted. Hence, a spatial age distribution similar to an age gradient is observed. There are some exceptions to this simple view, which arise as a consequence of galaxy interactions. Relatively young star clusters with a metallicity content of those formed in the LMC bar or inner disk were found in the outer LMC disk, where older and more metal-poor ones are expected to survive (Piatti 2016). Piatti et al. (2018a) showed that such objects could have been born in the innermost LMC regions and then scattered to the outer LMC disk. Ram pressure interaction between the LMC and the Milky Way and between both MCs could also triggered star cluster formation in the periphery of the MCs (Sitek et al. 2016; Piatti et al. 2018b), while some old globular clusters could be associated to the accreted satellite populations of the LMC (Martin et al. 2016; Cerny et al. 2020).

Within our studied star cluster sample, Field 4−01 is located in the so-called west halo of the SMC (Dias et al. 2014), a region placed on the opposite side of the bridge which was predicted by Diaz & Bekki (2012) models and most likely has a tidal origin linked to the dynamical history of the MCs. Most of the known star clusters grouped in this area are generally of intermediate-age or older (Dias et al. 2016), so that Field 4−01 can be now added to this group ($\log(\mathrm{age\,yr^{-1}}) = 9.45$). Below the onset of the Magellanic bridge and somehow superimposed to it (to the southeast from the SMC center), there is also a region of moderately old star clusters (Piatti et al. 2007a; Piatti 2011a,b). We estimated an age of 5.5 Gyr ($\log(\mathrm{age\,yr^{-1}}) = 9.74$)

Table 1. Fundamental parameters of Magellanic Cloud clusters.

Star cluster [(a)]	RA (deg)	Dec (deg)	r (arcmin)	$(m-M)_0$ (mag)	log(age yr^{-1})	[Fe/H] (dex)	Mass ($M_\odot$)	q
Field 4−01	8.254	−72.989	0.30	18.73 ± 0.22	9.47 ± 0.16	−0.97 ± 0.31	806 ± 626	0.44 ± 0.27
Field 10−01	16.895	−72.164	0.30	18.76 ± 0.24	7.54 ± 0.49	−0.92 ± 0.05	338 ± 297	0.39 ± 0.25
Field 10−02	18.098	−72.292	0.30	18.92 ± 0.29	8.27 ± 0.21	−0.53 ± 0.27	177 ± 38	0.51 ± 0.28
Field 10−03	16.194	−72.716	0.30	18.87 ± 0.36	8.11 ± 0.18	−0.43 ± 0.26	358 ± 147	0.51 ± 0.25
Field 11−01	15.982	−72.933	0.30	19.04 ± 0.37	7.87 ± 0.18	−0.52 ± 0.34	926 ± 586	0.53 ± 0.28
Field 11−02	15.325	−73.465	0.30	18.56 ± 0.34	8.15 ± 0.13	−0.44 ± 0.25	628 ± 250	0.53 ± 0.24
Field 11−03	16.048	−74.299	0.20	19.10 ± 0.26	8.96 ± 0.62	−0.71 ± 0.45	534 ± 341	0.52 ± 0.29
Field 12−01	18.427	−74.753	0.30	18.42 ± 0.24	9.74 ± 0.15	−0.98 ± 0.44	155 ± 44	0.54 ± 0.29
Field 15−01	20.753	−73.218	0.25	18.72 ± 0.21	8.05 ± 0.45	−0.80 ± 0.43	208 ± 85	0.37 ± 0.25
Field 16−01	22.471	−74.846	0.50	19.01 ± 0.15	9.09 ± 0.07	−0.53 ± 0.13	390 ± 58	0.53 ± 0.25
Field 16−02	22.461	−74.682	0.50	18.87 ± 0.31	9.19 ± 0.13	−0.83 ± 0.30	1085 ± 198	0.68 ± 0.19
Field 30−01	72.066	−69.672	0.30	18.58 ± 0.26	7.88 ± 0.39	−0.44 ± 0.27	238 ± 102	0.51 ± 0.28
Field 40−01	80.275	−71.913	0.30	18.64 ± 0.41	7.34 ± 0.41	−0.78 ± 0.18	601 ± 377	0.58 ± 0.30
Field 40−02	81.364	−72.639	0.30	18.42 ± 0.25	8.76 ± 0.25	−0.78 ± 0.37	186 ± 60	0.60 ± 0.28
Field 40−03	78.142	−72.626	0.40	18.52 ± 0.28	8.89 ± 0.27	−0.49 ± 0.28	116 ± 16	0.58 ± 0.28
Field 40−04	79.484	−73.557	0.30	18.62 ± 0.40	9.01 ± 0.23	−0.26 ± 0.17	213 ± 84	0.54 ± 0.29
Field 40−05	80.489	−73.513	0.50	18.40 ± 0.32	8.96 ± 0.16	−0.73 ± 0.17	215 ± 100	0.63 ± 0.26
Field 40−06	78.088	−73.270	0.30	18.83 ± 0.41	8.66 ± 0.17	−0.37 ± 0.23	254 ± 118	0.50 ± 0.29
Field 40−07	81.081	−73.091	0.30	18.69 ± 0.33	8.55 ± 0.72	−0.26 ± 0.15	342 ± 372	0.56 ± 0.28
Field 44−01	82.674	−75.668	0.30	18.50 ± 0.37	9.34 ± 0.25	−0.38 ± 0.24	389 ± 340	0.53 ± 0.29
Field 44−02	81.523	−75.416	0.25	18.42 ± 0.29	9.35 ± 0.21	−0.54 ± 0.22	217 ± 196	0.53 ± 0.28
Field 51−01	87.308	−70.6737	0.30	18.57 ± 0.26	7.87 ± 0.38	−0.78 ± 0.47	262 ± 122	0.55 ± 0.29
Field 55−01	96.733	−70.3008	0.20	18.56 ± 0.34	8.70 ± 0.29	−0.48 ± 0.18	154 ± 46	0.52 ± 0.28

Notes. Columns are: radius of the cleaned star cluster area (r); true distance modulus ($(m-M)_0$); age; metallicity ([Fe/H]); star cluster mass; and binary fraction (q). [(a)]Star cluster identifications are from Piatti (2017, Table 1).

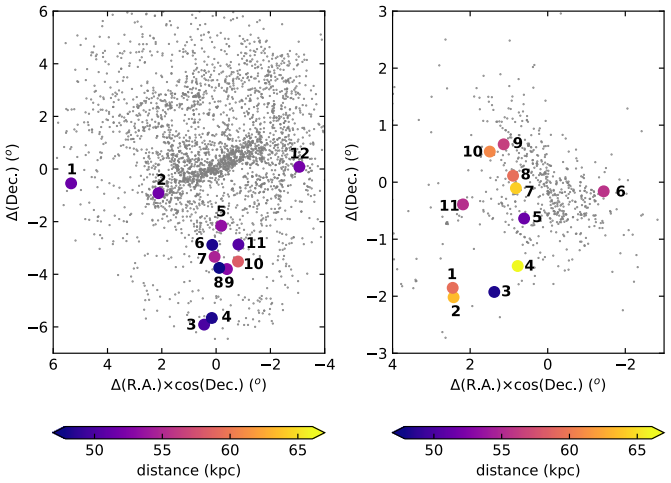

Fig. 5. Spatial distribution of the MC clusters. North is up and east to the left. Gray points are star clusters in the Bica et al. (2008)'s catalog, while color-coded large circles represent the studied star cluster sample. *Left LMC*: 1 = Field 55−01; 2 = Field 51−01; 3 = Field 44−01; 4 = Field 44−02; 5 = Field 40−01; 6 = Field 40−02; 7 = Field 40−06; 8 = Field 40−04; 9 = Field 40−05; 10 = Field 40−07; 11 = Field 40−03; 12 = Field 30−01. *Right SMC*: 1 = Field 16−02; 2 = Field 16−01; 3 = Field 12−01; 4 = Field 11−03; 5 = Field 11−02; 6 = Field 4−01; 7 = Field 11−01; 8 = Field 10−03; 9 = Field 10−01; 10 = Field 10−02; 11 = Field 15−01.

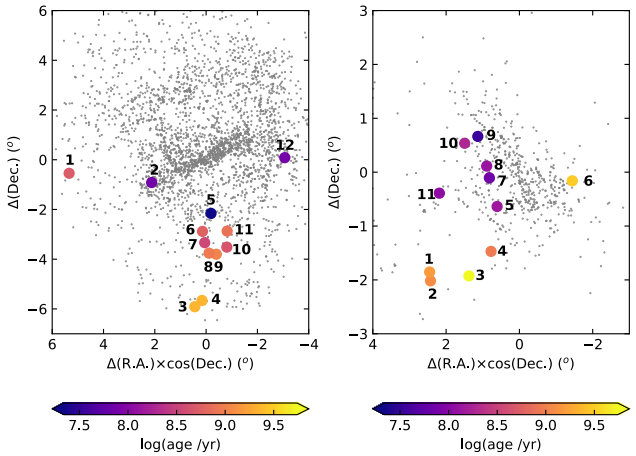

Fig. 6. Same as Fig. 5, color-coded according to the star cluster ages.

for Field 12−01 that matches the ages of this group of star clusters very well. Other two star clusters, Field 16−01 and 16−02, also located in this region, are a bit younger though (log(age yr^{-1}) ∼ 9.2). We note that Field 12−01 is located at the LMC distance, so that it could be a halo SMC star cluster affected by the LMC gravitational field (Carpintero et al. 2013). By using the elliptical framework devised by Piatti et al. (2007b) to reflect more meaningfully the flattening of the galaxy, the remaining studied SMC star clusters are located to the east of the SMC center at semi-major axes of ∼3° and beyond. They resulted to be young objects (age $\lesssim$ 200 Myr), with only one exception, Field 11−03 (log(age yr^{-1}) ∼ 9.0). While the older one is in agreement with the average age of star clusters in that region (log(age yr^{-1}) $\gtrsim$ 9.0 Dias et al. 2016), the younger one would seem more tightly related to the onset of the Magellanic bridge

(Piatti et al. 2015). As for the spatial distribution of ages of LMC star clusters, that of Field 55−01 (the easternmost star cluster in the studied sample) would seem to be characteristic of a likely runaway object (Piatti et al. 2018a), while the other star clusters agree with the presence of an age gradient; those farther from the LMC center being older.

The chemical enrichment of the MCs has long been studied from various theoretical and observational approaches. Some of the most recurrent age-metallicity relationships used in this field are the models computed by Pagel & Tautvaisiene (1998, PT98), which predict intensive star formation and chemical enrichment during the initial formation epoch that brought the metallicity up about −0.7 dex and −1.3 dex, for the LMC and SMC, respectively. This turbulent period was subsequently followed by relative quiescence period to finally be disturbed by rapid burst of chemical enrichment about 3 Gyr ago ($\log(\mathrm{age\,yr^{-1}}) \approx 9.5$), which brought the global metallicities up to their current values. Because of the coincidence in the ages of LMC and SMC star clusters formed at that time, it has been argued that the bursting formation events were caused by the interaction between both MCs (Piatti 2011a,c, 2012). Bekki & Tsujimoto (2012, BT12) also presented a bursting model for the LMC with some different ingredients. The closed-box model of chemical evolution presented by Geha et al. (1998, hereafter G98) and Da Costa & Hatzidimitriou (1998, hereafter closed-box) a predicted gradual increase of star formation and metal abundances over time. The major merger scenario for the SMC was proposed by Tsujimoto & Bekki (2009, TB09). The model predicts that major merger occurred ≈7.5 Gyr ago and was calculated for three cases: no merger (TB09-01), one-to-one merger (TB09-02), and one-to-four merger (TB09-03). From an observational point of view, Harris & Zaritsky (2009, HZ09) and Harris & Zaritsky (2004, HZ04) built age-metallicity relationships for the LMC and SMC, respectively, based on *UBVI* photometry from the Magellanic Clouds Photometric Survey, while Piatti & Geisler (2013, PG13) constructed the age-metallicity relations for LMC and SMC star clusters using Washington photometry.

Figure 7 shows the above-listed age-metallicity relations for the MCs with the present studied star clusters superimposed. They span a quite wide range of ages, from very young star clusters ($\log(\mathrm{age\,yr^{-1}}) \sim 7.5$) up to intermediate-age ones ($\log(\mathrm{age\,yr^{-1}}) \sim 9.5$). In the LMC, none of the discovered star clusters turned out to be older than ∼2.5 Gyr ($\log(\mathrm{age\,yr^{-1}}) \approx 9.4$), which is in agreement with the general consensus of the existence of a star cluster age gap in the LMC, from ∼4 Gyr ($\log(\mathrm{age\,yr^{-1}}) \approx 9.6$) up to the oldest globular clusters' ages (Olszewski et al. 1991; Rich et al. 2001; Piatti et al. 2009; Piatti & Geisler 2013). The metallicities of the LMC and SMC star clusters are within the theoretically predicted and observed boundaries. Perhaps, the most noticeable feature is the existence of young star clusters (age $\lesssim$ 100 Myr) with relatively low metal content in both MCs ([Fe/H] ∼ −0.7 dex), similar to ∼1 Gyr old ($\log(\mathrm{age\,yr^{-1}}) \approx 9.0$) metal-poor star clusters. This might imply that a relatively metal-deficient gaseous flow could have existed between both MCs over the last few Gyr, which is also responsible for the Magellanic Stream and Leading Arm and triggered star cluster formation (Ruiz-Lara et al. 2020; Tsuge et al. 2020). On the other hand, chemical enhancement has reached slightly different metallicity levels. The iron-to-hidrogen ratios increased on average up to -0.30 ± 0.15 dex and -0.50 ± 0.20 dex, in the LMC and SMC, respectively. The present results illustrate that the MCs are more complex galactic systems than previously known. The consideration of initial galaxy formation and later interactions between them and with the Milky Way guide us towards a better understanding of their present age and metallicity distributions of star clusters throughout the entire Magellanic system.

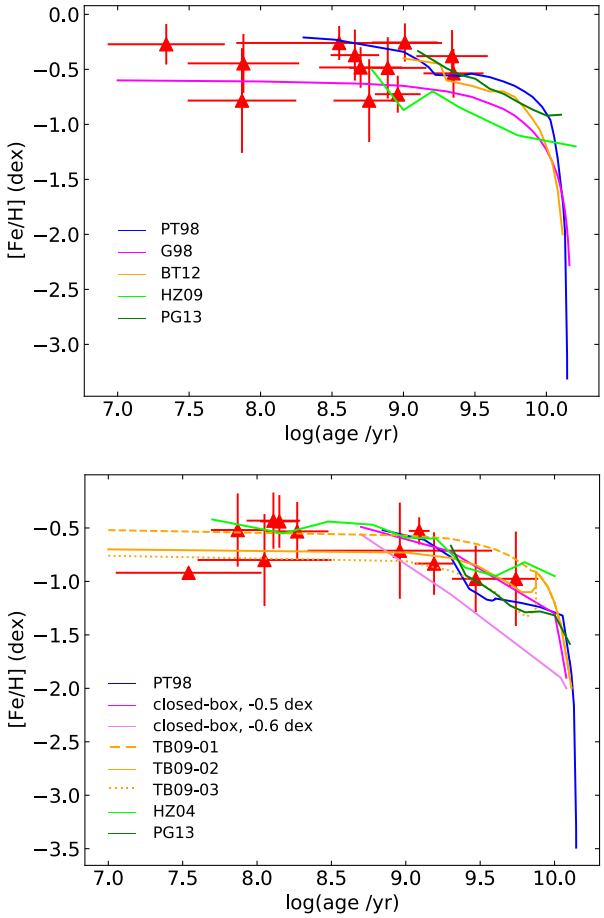

Fig. 7. Age-metallicity relationships for the LMC (*top panel*) and SMC (*bottom panel*). Triangles represent star clusters studied in this work (error bars included, see Table 1), while the colored lines correspond to different theoretical or observed age-metallicity relationships: Pagel & Tautvaisiene (1998, PT98), Geha et al. (1998, G98), Bekki & Tsujimoto (2012, BT12), Harris & Zaritsky (2009, HZ09), Piatti & Geisler (2013, PG13), Da Costa & Hatzidimitriou (1998, closed-box), Tsujimoto & Bekki (2009, TB09), and Harris & Zaritsky (2004, HZ04).

4. Concluding remarks

We conducted analyses to obtain fundamental parameters estimates of 24 Magellanic Cloud star cluster candidates recently discovered by Piatti (2017) using the SMASH DR2 database. We find that all candidates have turned out to be genuine physical systems, with the sole exception of one candidate called Field 30−02. We were able to arrive at such a conclusion once the observed star cluster CMDs were carefully decontaminated from field stars and the cleaned CMDs were compared to synthetic CMDs generated for thousand combinations of ages, distances, metallicities, star cluster mass, and binary fractions. The parameter of the best-matched synthetic CMDs obtained from a likelihood approach were adopted as the star cluster astrophysical properties. In making the comparison between observed and synthetic CMDs, we only used stars that passed the cleaning procedure and were assigned membership probabilities higher than

50%. The use of a parallel tempering Bayesian MCMC algorithm to explore the multi-parameter space allowed us to avoid typical constraints of adopting mean Magellanic Cloud distances and metallicities in studies of star clusters. Those assumptions provided us with a limited picture of the MCs, where extended halos and tidally distorted peripheries are not distinguished.

Indeed, the present star cluster sample spans a wide range of distances, from those star clusters located behind the SMC, going through those placed in between both MCs along the Magellanic bridge, to those in from of the LMC. Such a spatial distribution is, independently, a witness of interaction between both MCs. Their estimated ages also tell us about the varied mixture of formation episodes. Some clusters were born according to the outside-in formation scenario, where older star clusters are more commonly seen in outer galaxy regions (Gallart et al. 2008; Carrera et al. 2011). However, because of the interaction among the MCs themselves and the interaction among the MCs and the Milky Way, gas flows could have existed, initially feeding the outer regions where young star cluster formed out of them. We find evidence of such formation phenomenon based on the identification of star clusters with different ages populating the same galaxy region and star clusters that are found to be projected toward regions with associated stellar ages and metallicities different from those of the star clusters. The estimated ages and metallicities confirm the general accepted evolution of the chemical enrichment in the MCs. From the estimated star cluster metallicities, we find another indicator of the existence of gaseous flows between these galaxies. There are very young clusters ($\sim$30 Myr) in both MCs, located in their outer regions, with metal abundances as deficient as the most metal-poor star clusters with ages $\lesssim 1$ Gyr ($\log(\text{age yr}^{-1}) \approx 9.0$). The most metal-rich young star clusters have slightly different [Fe/H] values, with those of the LMC being more metal-rich.

Comparing the present-day masses of the studied star clusters with those of Milky Way open clusters with similar ages located in the solar neighborhood (distance to the Sun < 1.8 kpc, Joshi et al. 2016), we find that the studied Magellanic Cloud clusters are generally similar or more massive than open clusters. Their binary frequencies are, on average, $q = 0.55$, a value that is independent of the star cluster mass.

Acknowledgements. I thank the referee for the thorough reading of the manuscript and timely suggestions to improve it. This research uses services or data provided by the Astro Data Lab at NSF's National Optical-Infrared Astronomy Research Laboratory. NSF's OIR Lab is operated by the Association of Universities for Research in Astronomy (AURA), Inc. under a cooperative agreement with the National Science Foundation.

References

Abbott, T. M. C., Abdalla, F. B., Allam, S., et al. 2018, ApJS, 239, 18
Bekki, K., & Tsujimoto, T. 2012, ApJ, 761, 180
Bica, E., Bonatto, C., Dutra, C. M., & Santos, J. F. C. 2008, MNRAS, 389, 678
Bica, E., Westera, P., Kerber, L. D. O., et al. 2020, AJ, 159, 82
Bressan, A., Marigo, P., Girardi, L., et al. 2012, MNRAS, 427, 127
Carpintero, D. D., Gómez, F. A., & Piatti, A. E. 2013, MNRAS, 435, L63
Carrera, R., Gallart, C., Aparicio, A., et al. 2008, AJ, 136, 1039
Carrera, R., Gallart, C., Aparicio, A., & Hardy, E. 2011, AJ, 142, 61
Cerny, W., Pace, A. B., Drlica-Wagner, A., et al. 2020, AAS J., submitted [arXiv:2009.08550]
Choi, Y., Nidever, D. L., Olsen, K., et al. 2018, ApJ, 866, 90
Crowl, H. H., Sarajedini, A., Piatti, A. E., et al. 2001, AJ, 122, 220
Da Costa, G. S., & Hatzidimitriou, D. 1998, AJ, 115, 1934
de Grijs, R., Wicker, J. E., & Bono, G. 2014, AJ, 147, 122
Dias, B., Kerber, L. O., Barbuy, B., et al. 2014, A&A, 561, A106
Dias, B., Kerber, L., Barbuy, B., Bica, E., & Ortolani, S. 2016, A&A, 591, A11
Diaz, J. D., & Bekki, K. 2012, ApJ, 750, 36
Efron, B. 1982, The Jackknife, the Bootstrap and Other Resampling Plans
Gaia Collaboration (Prusti, T., et al.) 2016, A&A, 595, A1
Gaia Collaboration (Brown, A. G. A., et al.) 2018, A&A, 616, A1
Gallart, C., Stetson, P. B., Meschin, I. P., Pont, F., & Hardy, E. 2008, ApJ, 682, L89
Gatto, M., Ripepi, V., Bellazzini, M., et al. 2020, MNRAS, 499, 4114
Geha, M. C., Holtzman, J. A., Mould, J. R., et al. 1998, AJ, 115, 1045
Graczyk, D., Pietrzynski, G., Thompson, I. B., et al. 2020, ApJ, 904, 13
Harris, J., & Zaritsky, D. 2004, AJ, 127, 1531
Harris, J., & Zaritsky, D. 2009, AJ, 138, 1243
Jacyszyn-Dobrzeniecka, A. M., Skowron, D. M., Mróz, P., et al. 2017, Acta Astron., 67, 1
Joshi, Y. C., Dambis, A. K., Pandey, A. K., & Joshi, S. 2016, A&A, 593, A116
Kroupa, P. 2002, Science, 295, 82
Mackey, A. D., Koposov, S. E., Erkal, D., et al. 2016, MNRAS, 459, 239
Mackey, A. D., Koposov, S. E., Da Costa, G. S., et al. 2017, MNRAS, 472, 2975
Maia, F. F. S., Dias, B., Santos, J. F. C., et al. 2019, MNRAS, 484, 5702
Martin, N. F., Jungbluth, V., Nidever, D. L., et al. 2016, ApJ, 830, L10
Massana, P., Noël, N. E. D., Nidever, D. L., et al. 2020, MNRAS, 498, 1034
Meschin, I., Gallart, C., Aparicio, A., et al. 2014, MNRAS, 438, 1067
Nidever, D. L., Olsen, K., Walker, A. R., et al. 2017, AJ, 154, 199
Nidever, D. L., Olsen, K., Choi, Y., et al. 2019, ApJ, 874, 118
Olszewski, E. W., Schommer, R. A., Suntzeff, N. B., & Harris, H. C. 1991, AJ, 101, 515
Pagel, B. E. J., & Tautvaisiene, G. 1998, MNRAS, 299, 535
Perren, G. I., Vázquez, R. A., & Piatti, A. E. 2015, A&A, 576, A6
Piatti, A. E. 2011a, MNRAS, 418, L69
Piatti, A. E. 2011b, MNRAS, 416, L89
Piatti, A. E. 2011c, MNRAS, 418, L40
Piatti, A. E. 2012, MNRAS, 422, 1109
Piatti, A. E. 2016, MNRAS, 459, L61
Piatti, A. E. 2017, ApJ, 834, L14
Piatti, A. E. 2018a, MNRAS, 478, 784
Piatti, A. E. 2018b, MNRAS, 477, 2164
Piatti, A. E., & Bica, E. 2012, MNRAS, 425, 3085
Piatti, A. E., & Geisler, D. 2013, AJ, 145, 17
Piatti, A. E., Sarajedini, A., Geisler, D., Gallart, C., & Wischnjewsky, M. 2007a, MNRAS, 381, L84
Piatti, A. E., Sarajedini, A., Geisler, D., Clark, D., & Seguel, J. 2007b, MNRAS, 377, 300
Piatti, A. E., Geisler, D., Sarajedini, A., & Gallart, C. 2009, A&A, 501, 585
Piatti, A. E., Guandalini, R., Ivanov, V. D., et al. 2014, A&A, 570, A74
Piatti, A. E., de Grijs, R., Rubele, S., et al. 2015, MNRAS, 450, 552
Piatti, A. E., Ivanov, V. D., Rubele, S., et al. 2016, MNRAS, 460, 383
Piatti, A. E., Salinas, R., & Grebel, E. K. 2018a, MNRAS, 482, 980
Piatti, A. E., Cole, A. A., & Emptage, B. 2018b, MNRAS, 473, 105
Piatti, A. E., Alfaro, E. J., & Cantat-Gaudin, T. 2019, MNRAS, 484, L19
Piatti, A. E., Carballo-Bello, J. A., Mora, M. D., et al. 2020, A&A, 643, A15
Rich, R. M., Shara, M. M., & Zurek, D. 2001, AJ, 122, 842
Ruiz-Lara, T., Gallart, C., Monelli, M., et al. 2020, A&A, 639, L3
Sitek, M., Szymański, M. K., Skowron, D. M., et al. 2016, Acta Astron., 66, 255
Subramanian, S., & Subramaniam, A. 2009, A&A, 496, 399
Tremmel, M., Fragos, T., Lehmer, B. D., et al. 2013, ApJ, 766, 19
Tsuge, K., Sano, H., Sano, K., et al. 2020, ApJ, submitted [arXiv:2010.08816]
Tsujimoto, T., & Bekki, K. 2009, ApJ, 700, L69
Wagner-Kaiser, R., & Sarajedini, A. 2017, MNRAS, 466, 4138

Appendix A: Fundamental parameters of star clusters

In this section, we present the results of the cleaning procedure applied to the analyzed star cluster CMDs in order to decontaminate them from the star field contamination, similarly as presented in Fig. 4 (see, Figs. A.1–A.6). Details about the estimation of the star cluster astrophysical properties are also described in Sect. 2.

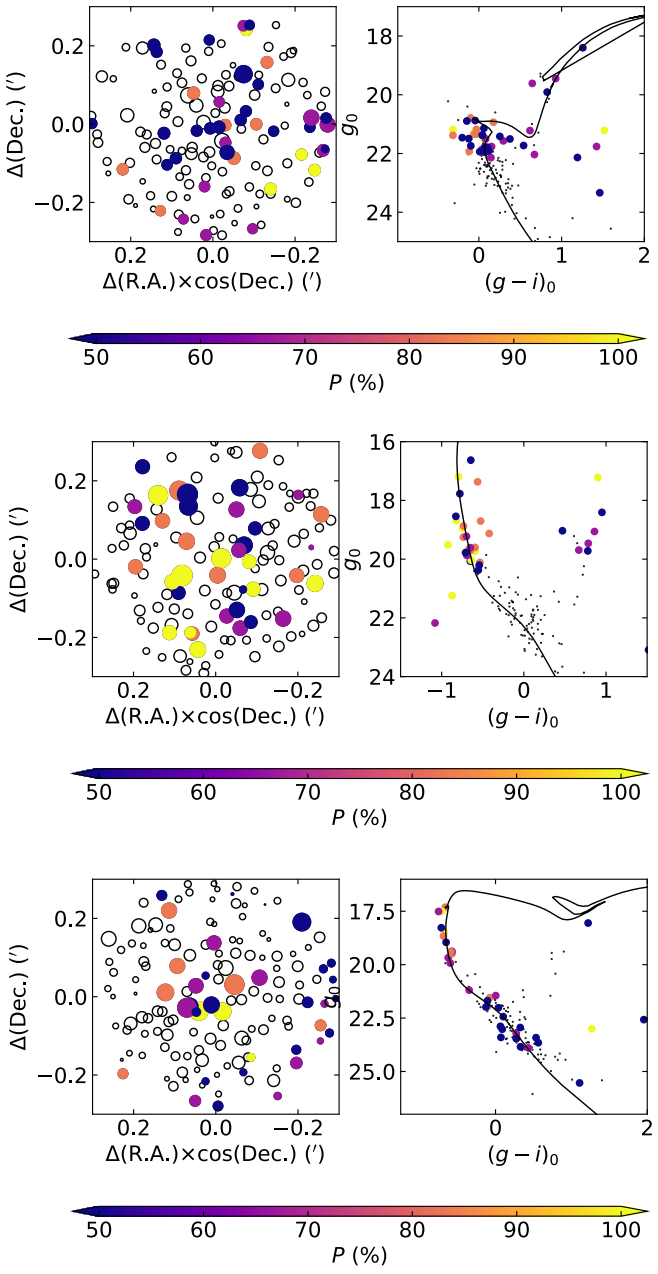

Fig. A.1. Same as Fig. 4 for Field 4−01, 10−01, and 10−02.

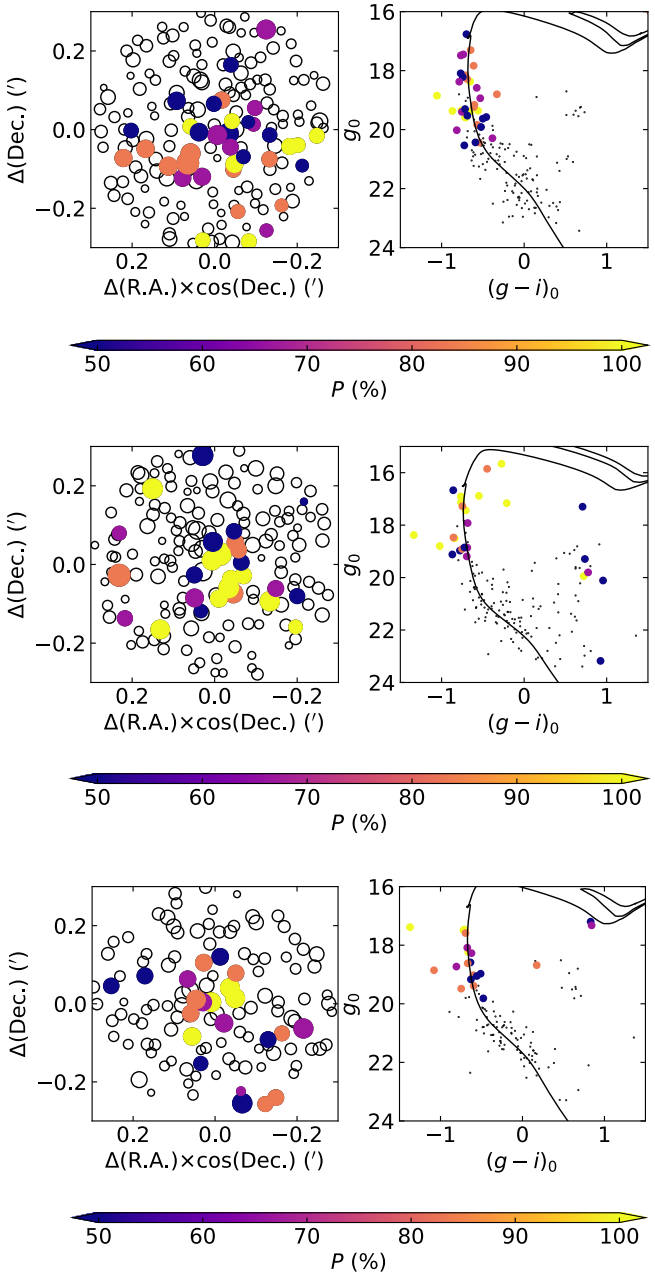

Fig. A.2. Same as Fig. 4 for Field 10−03, 11−01, and 11−02.

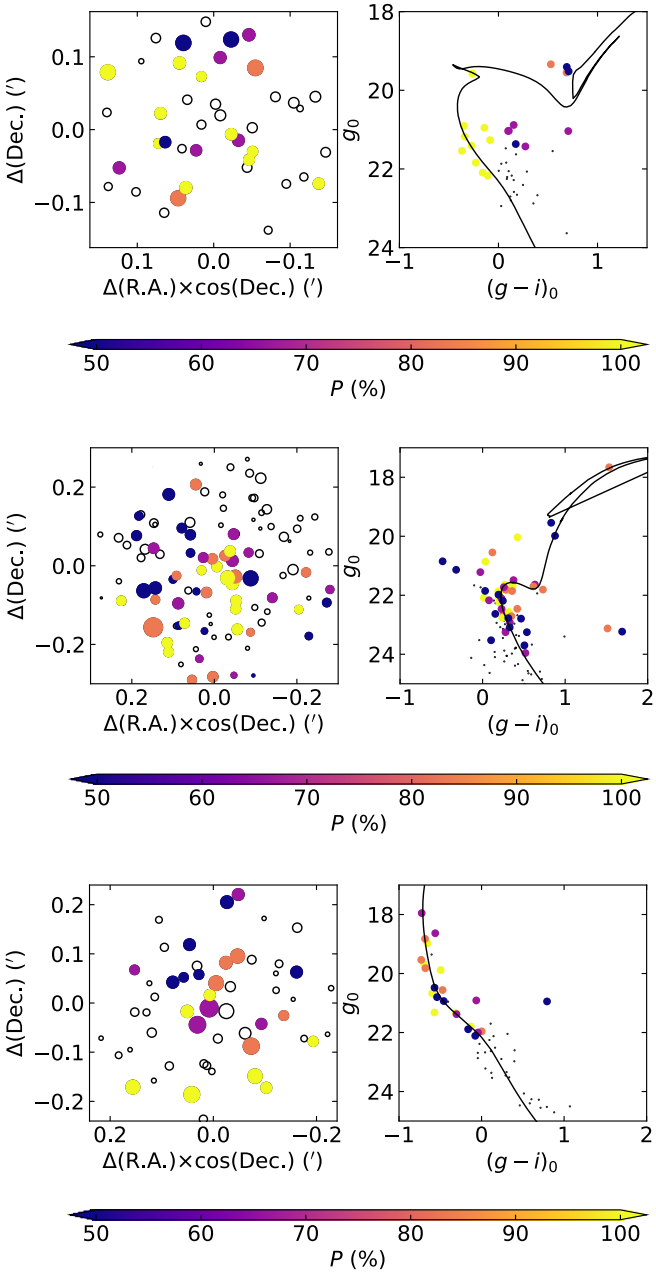

Fig. A.3. Same as Fig. 4 for Field 11−03, 12−01, and 15−01.

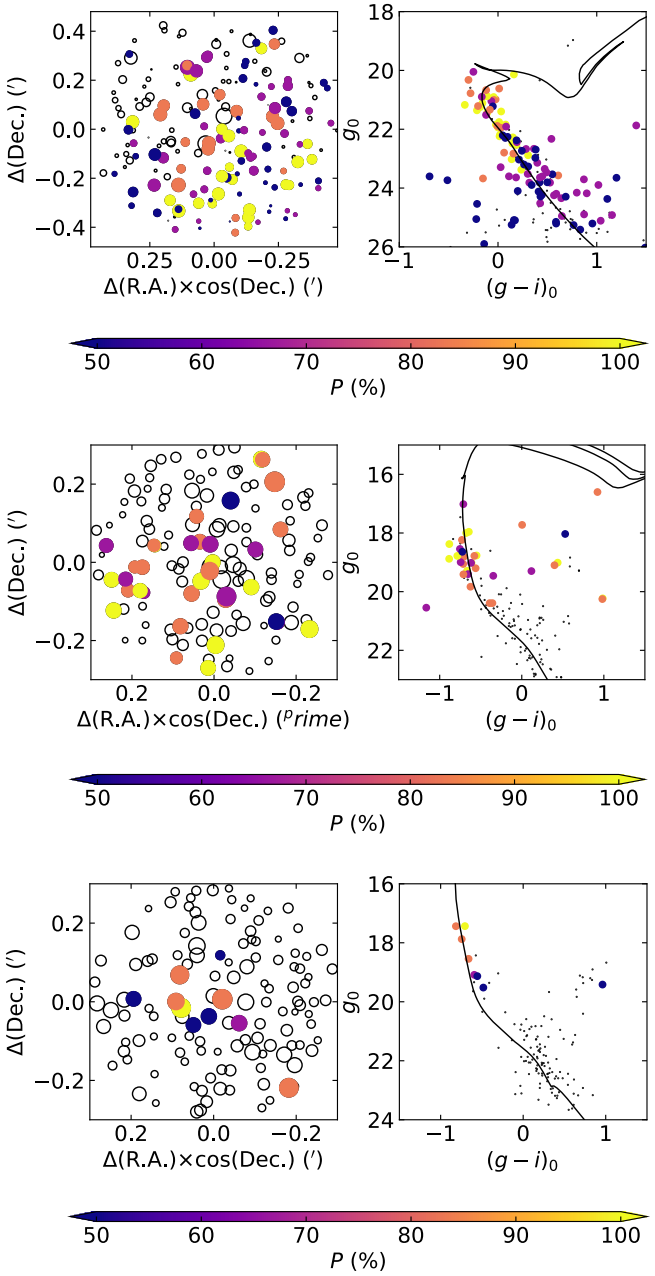

Fig. A.4. Same as Fig. 4 for Field 16−01, 30−01, and 40−01.

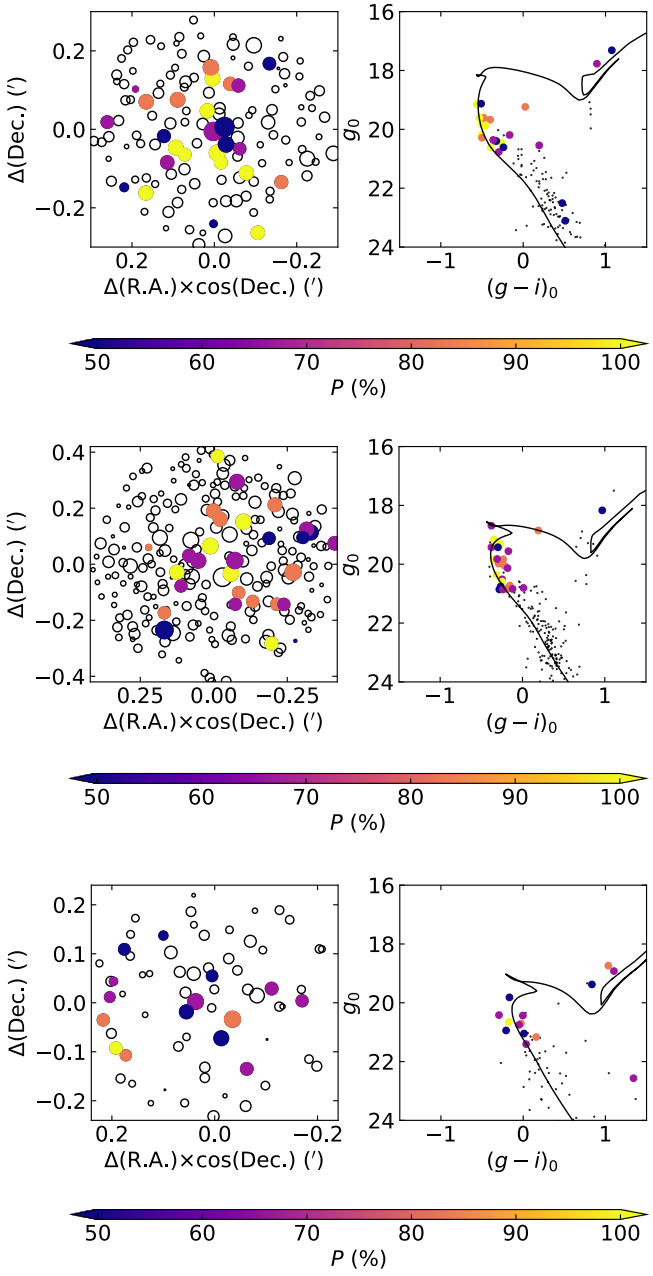

Fig. A.5. Same as Fig. 4 for Field 40−02, 40−03, and 40−04.

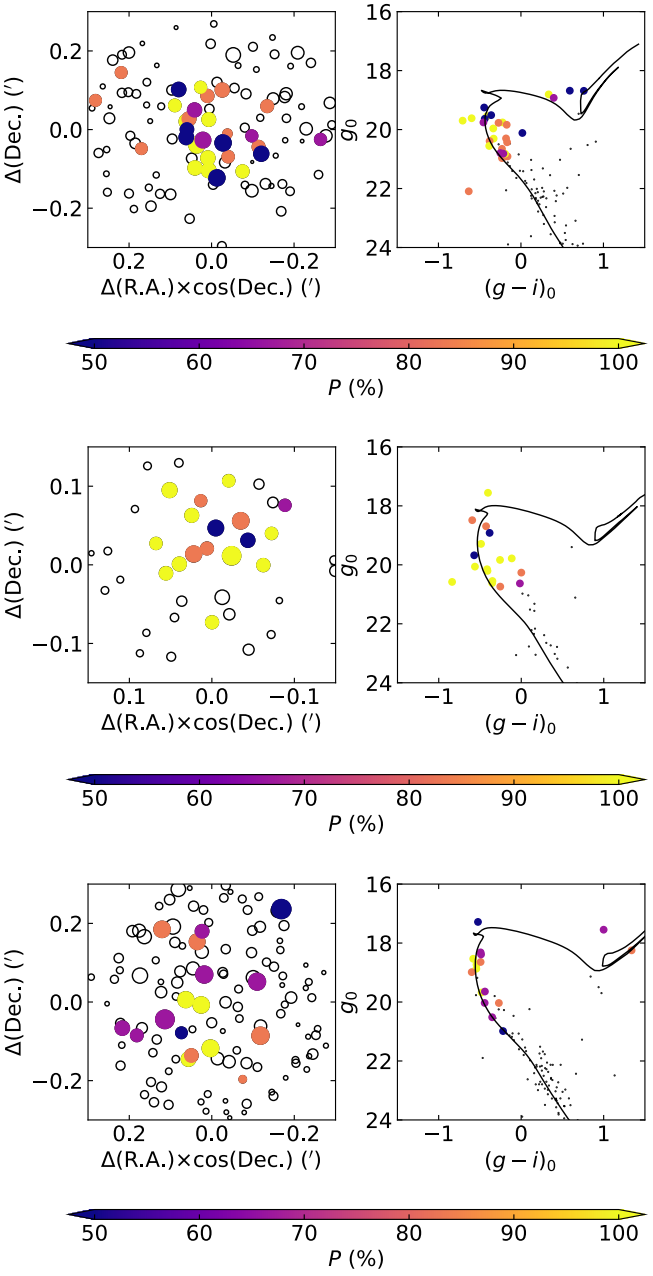

Fig. A.6. Same as Fig. 4 for Field 40−05, 40−06, and 40−07.

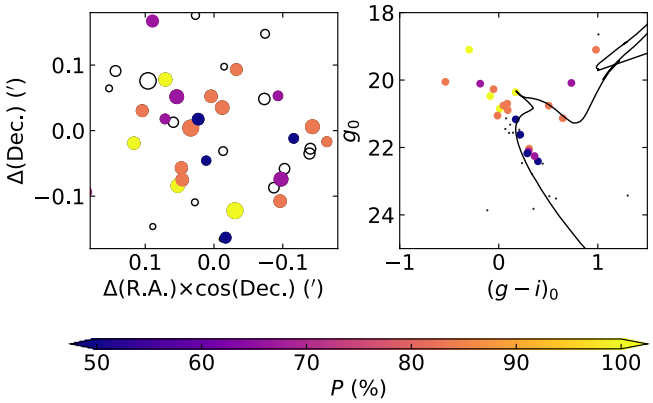

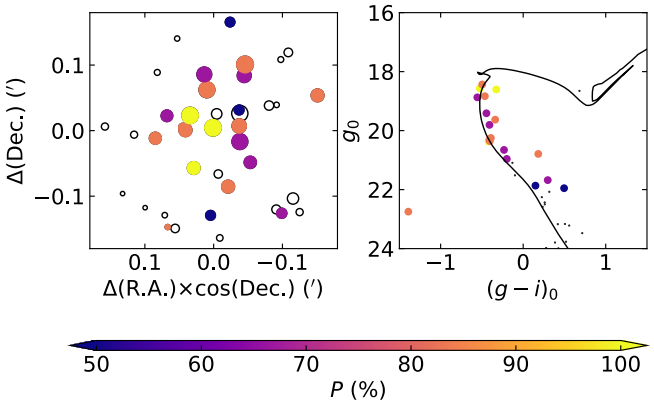

Fig. A.8. Same as Fig. 4 for Field 55−01.

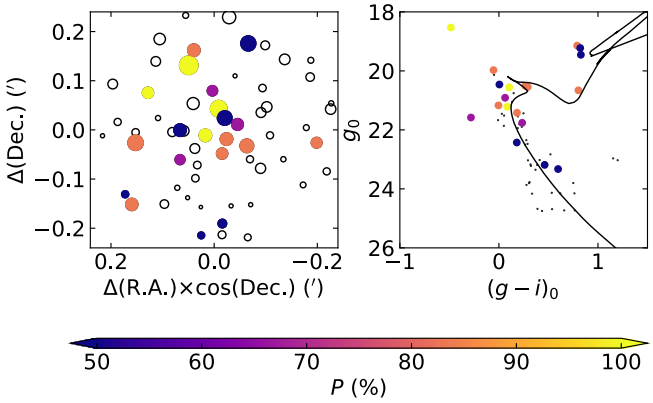

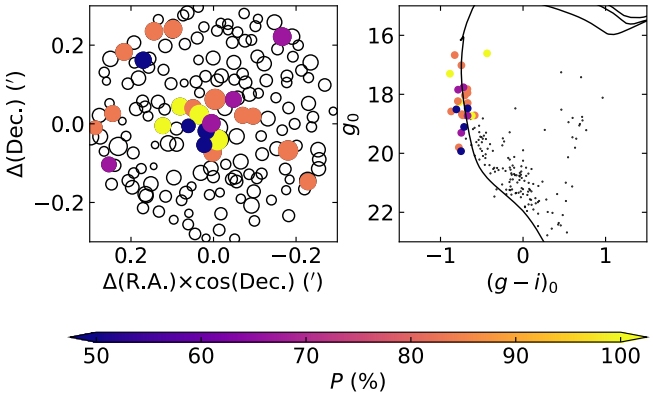

Fig. A.7. Same as Fig. 4 for Field 44−01, 44−02, and 51−01.